Encapsulation of Pt Nanoparticles as a Result of Strong Metal−Support Interaction with Fe_3O_4 (111)

Z.-H. Qin, M. Lewandowski, Y.-N. Sun, S. Shaikhutdinov,* and H.-J. Freund

Department of Chemical Physics, Fritz-Haber Institute of the Max Planck Society, Faradayweg 4-6, Berlin 14195, Germany

Received: February 28, 2008; Revised Manuscript Received: March 31, 2008

The morphology and thermal stability of Pt particles deposited on Fe_3O_4 (111) films were studied by scanning tunneling microscopy (STM) and temperature programmed desorption of CO. Vacuum annealing at temperatures above 800 K led to significant Pt sintering that reduced CO uptake to a much higher extent than the Pt surface area. A similar effect on CO adsorption was observed after mild oxidation−reduction treatment at 500 K. The results are rationalized in terms of the strong metal−support interaction between Pt and Fe_3O_4, whereby the Pt particles were encapsulated by a FeO (111) monolayer film as shown by STM. The high adhesion energy between Pt and iron oxides derived from STM data is suggested to be the key factor for encapsulation.

Introduction

Strong metal−support interactions (SMSI) were originally developed as an explanation for the decreased chemisorption of CO and H_2 on metal particles supported on reducible metal oxides.[1] Different models were proposed, such as alloy formation, electronic interactions, and, in most cases, encapsulation or decoration of the metal by the oxide (see refs 1–5 and references therein).

It is generally accepted that minimization of surface energy is one of the main driving forces for encapsulation. As pointed out by Taglauer and Knözinger,[6] oxides with a relatively low surface energy (such as titania, ceria, and vanadia) undergo the SMSI effect, while alumina and silica do not. In turn, metals having a relatively high surface energy (such as Pt, Rh, and Pd but not Ag and Cu) favor encapsulation.

To gain a deeper understanding of these phenomena, model studies have been suggested, in which metal particles are supported on oxide single crystals or thin, well-ordered oxide films. Madey and co-workers[7–9] studied the interaction of metals with TiO_2 (110) and found encapsulation of Fe, Pd, and Pt (but not Au) particles upon heating in a vacuum. According to the results of Suzuki and Souda,[10] the crystal structure of the Pd islands and the Pd/TiO_2 (110) interface remained unchanged during the encapsulation, thus suggesting that encapsulation proceeds through mass transport along the surface and not through the metal particle. Using scanning tunneling microscopy (STM), Diebold's and Bowker's groups provided direct evidence for encapsulation of Pt[11,12] and Pd[13–15] particles by a TiO_x thin layer, although there is still debate on as to whether the overlayer is an intermetallic-like alloy or a complete titania layer (see also refs 16 and 17).

Mullins et al., using temperature programmed desorption (TPD) of CO and photoelectron spectroscopy, found encapsulation of Pt (and not Pd) particles supported on reduced but not on oxidized CeO_2 (111) thin films.[18,19] This is consistent with the view of Gao et al.,[20] based on their studies of Pt on Nb-doped TiO_2 (100) epitaxial films, that a high oxygen vacancy density in the oxide bulk is essential for encapsulation that involves oxygen diffusion. The influence of the electronic structure of TiO_2 (110) on encapsulation was addressed by Fu et al.,[21,22] who showed that interfacial space charges may strongly affect this process through Schottky-type band bending between metal and semiconductor, in turn depending on the work functions of the metal and oxide support.

Less is known about the interaction of platinum group metals with iron oxide surfaces. To the best of our knowledge, iron oxides were not reported for the SMSI effect. Epitaxial growth of Pt, Ag, and Au on oxide supported Fe_3O_4 films was studied by high energy electron diffraction and TEM.[23,24] The structure and reactivity of Pd particles on well-ordered Fe_3O_4 (111) film surfaces were studied in our own laboratories.[25–29] In particular, the formation of an interface oxide layer between Pd and Fe_3O_4 was observed upon oxidation at 500−550 K, which influences the kinetics of the CO oxidation reaction.

In this work, we present a combined STM and CO TPD study of Pt particles supported on Fe_3O_4 (111) films, which provides strong evidence for the encapsulation of Pt particles by a FeO (111) monolayer upon vacuum annealing at elevated temperatures. The high work of adhesion between Pt and iron oxides derived from STM data is suggested to be the key factor for encapsulation.

Experimental Section

The experiments were performed in an ultrahigh vacuum (UHV) chamber (base pressure below 10^{-10} mbar) equipped with low energy diffraction/Auger electron spectrometer (LEED/AES, Specs), STM, and differentially pumped quadrupole mass spectrometry (QMS). The Pt (111) crystal, mounted on a Pt sample holder, can be heated to 1300 K by electron bombardment from the backside using a tungsten filament. The temperature was controlled using a chromel−alumel thermocouple spot-welded to the edge of the crystal. A temperature ramp for TPD measurements was performed with a temperature control system (Schlichting Phys. Instrum.).

Iron and Pt (both 99.95%, Goodfellow) were vapor deposited using commercial evaporators (Focus EFM3, Omicron). During deposition, the sample was biased with a retarding potential to

* Corresponding author. E-mail: shaikhutdinov@fhi-berlin.mpg.de.

10.1021/jp801756q CCC: $40.75
Published on Web 05/29/2008

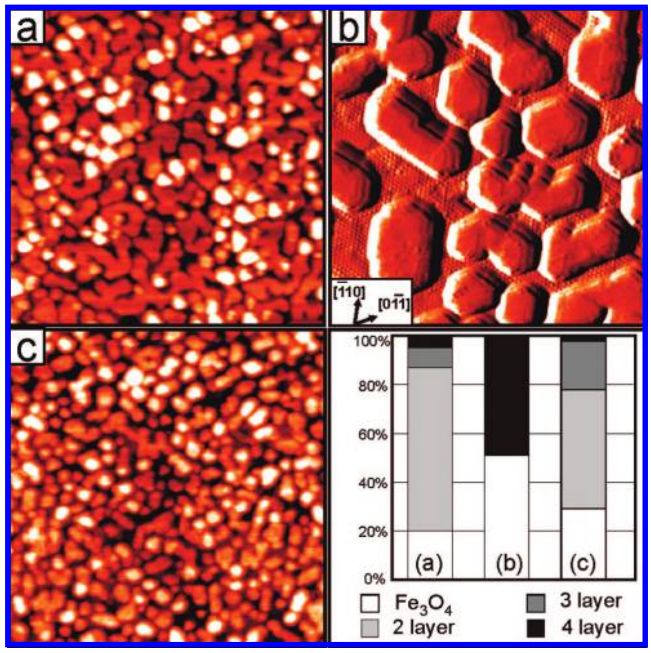

Figure 1. Room temperature STM images of 1.8 ML Pt/Fe_3O_4 (111) after annealing to 600 K (a) and 800 K (b). Image c shows an identically prepared sample as in image a, followed by oxidation−reduction treatment at 500 K (540 L of O_2 and 230 L of H_2) 1 L (Langmuir) = 10^{-6} Torr × sec). Image b is presented with a differentiated contrast. Crystallographic directions of the support are indicated. Size and tunneling parameters were (a) 100 nm × 100 nm, 0.7 V, and 0.4 nA; (b) 50 nm × 50 nm, 0.5 V, and 0.7 nA; and (c) 100 nm × 100 nm, 0.45 V, and 0.6 nA. The diagram shows the particles' height distribution in equivalent Pt (111) layers (one layer is 0.25 nm in height) and the fraction of the uncovered oxide surface for the samples imaged in images a−c.

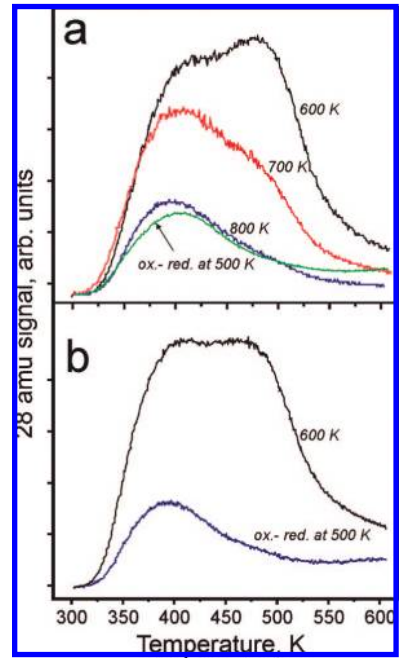

Figure 2. TPD spectra of CO on 1.8 ML Pt/Fe_3O_4(111). (a) The sample was stepwise annealed to 600, 700, and 800 K as indicated and then treated sequentially with 540 L of O_2 and 230 L of H_2 at 500 K. (b) The sample was annealed to 600 K and then subjected to oxidation−reduction treatment at 500 K. Twenty Langmuirs of CO was adsorbed at 300 K in each spectrum. The heating rate was 3 K/s.

prevent metal ions from being accelerated toward the sample. CO and hydrogen (99.995%, Linde) were exposed to the samples with a calibrated directional gas doser. High temperature oxidation was performed by back-filling the chamber with O_2 (99.999%, AGA GmbH).

The Fe_3O_4 (111) films were grown on a Pt (111) substrate as described in details in refs 30–32. About one monolayer (ML) of Fe was evaporated onto clean Pt (111) at 300 K and subsequently oxidized in 10^{-6} mbar O_2 at 1000 K for 2 min to form the FeO (111) monolayer film. The ~10 nm thick Fe_3O_4 (111) films were grown by repeated cycles of ~5 ML Fe deposition and oxidation at ~900 K with the final oxidation step at ~1000 K. After reaching UHV conditions prior to Pt deposition, the Fe_3O_4 (111) films were flashed to >800 K, resulting in a single termination oxide surface as judged by STM with large terraces up to 100 nm in width. Platinum was deposited onto these films at room temperature.

Results and Discussion

Figure 1a shows a typical STM image of the Pt/Fe_3O_4 (111) surface that was annealed to 600 K to combine STM and CO TPD results. (The samples were flashed to 600 K to desorb molecules (mainly CO), which may adsorb from the vacuum background during Pt deposition.) Platinum forms extended two-dimensional (2-D) islands of ~0.5 nm in thickness that exhibit mostly an irregular shape, although some preferential orientation for the island edges can be seen. At the metal coverage studied (~1.8 ML), 3-D particles also can be formed.

The corresponding CO TPD spectrum for this sample is shown in Figure 2a. Note that CO on the clean Fe_3O_4 (111) support desorbs at temperatures below 230 K[25,32] and therefore does not contribute to the spectra. On the basis of the Pt single crystal studies, CO desorption peaks at ~410 and ~480 K can be assigned to CO adsorbing on terraces and low coordination sites (such as steps, kinks, and particle edges), respectively.[33–36]

Stepwise annealing to 700 and 800 K in UHV leads to a dramatic reduction of the CO uptake, with preferential suppression of the high temperature desorption peak. This effect could be assigned to particle sintering at elevated temperatures. Indeed, Figure 1b shows that the particles size increases after annealing to 800 K so that the fraction of an uncovered substrate surface increases from ~20 to ~50%, on average (see the diagram in Figure 1). Interestingly, these annealed Pt particles are almost exclusively 0.9 ± 0.1 nm in height, a value that corresponds to four Pt (111) layers. In addition, the particles are well-faceted, with particle edges running along the main crystallographic directions on the Fe_3O_4 (111) surface (such as [$\bar{1}$10] and [01$\bar{1}$]), which can be deduced from atomic resolution between the particles (see Figure 1b). These results confirm the epitaxial relationship Pt (111) [1$\bar{1}$0]//Fe_3O_4 (111) [1$\bar{1}$0] found by diffraction methods,[23] whereby the particles expose the top (111) facets.

Analysis of the particles' height histogram and their perimeter length revealed that, after annealing to 800 K, the total Pt surface area was reduced by ~30%. Assuming that the adsorption of CO is not much affected by the precise morphology of the Pt particles and is proportional to the Pt surface area, at least for relatively large particles (>5 nm, see Figure 1), this would lead to the adsorption capacity decreasing by the same 30% upon annealing from 600 to 800 K. However, based on the TPD results shown in Figure 2a, CO uptake in fact decreased by 70% (i.e., much more than expected on the basis of particle sintering). Therefore, the combined STM and TPD results clearly point to SMSI between Pt and Fe_3O_4 (111).

There are no features in the presented TPD spectra that would be indicative of substantial Pt−Fe alloying. Indeed, the blank

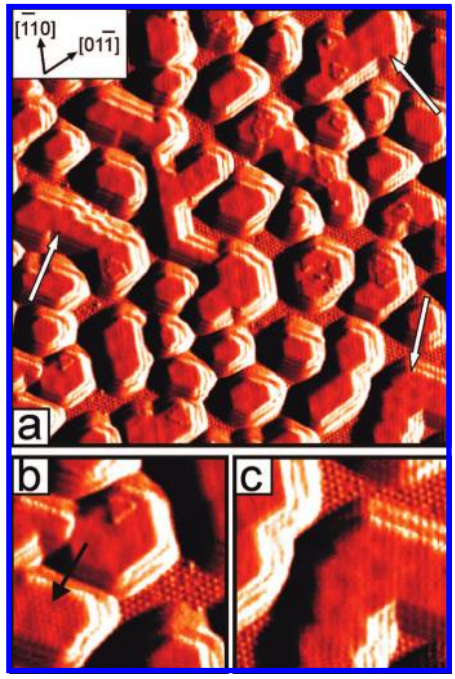

Figure 3. (a) STM image (80 nm × 80 nm, 0.5 V, and 0.6 nA) of 1.8 ML Pt/Fe_3O_4 (111) exposed to 540 L of O_2 at 500 K and flashed to 850 K in UHV. The arrows indicate some of the top facets where the Moiré superstructure is clearly seen, as enlarged in image c. The Pt particle showing a structure with ∼6 Å periodicity is shown in image b (size 20 nm × 20 nm).

experiments with Fe deposited onto the Pt (111) crystal surface reveal that the CO desorption shifts to the lower temperatures with increasing Fe coverage. Therefore, we conclude that the Pt particles are encapsulated by iron oxide under reducing conditions (vacuum) and that the decoration likely begins at the particle edges since CO adsorption on low coordination sites (i.e., high temperature peak in TPD) attenuates first (see Figure 2a). To see whether oxidative treatments also lead to a similar effect, the sample annealed to 600 K was first exposed to 10^{-6} mbar of O_2 (∼540 L) at 500 K and then to 10^{-6} mbar of H_2 (∼230 L) at the same temperature to remove oxygen from the Pt surface.

The STM image in Figure 1c shows less pronounced sintering. The uncovered support area increased from ∼20 to ∼30%, and a slight increase in the population of the 3- and 4-layer Pt particles was observed (see diagram in Figure 1). Overall, the Pt surface area estimated from the analysis of the STM images decreased by ∼25%, on average, as compared to the sample annealed to 600 K. However, CO uptake measured by TPD (Figure 2b) reduced by ∼75%, 3 times more than the Pt surface area. Therefore, the oxidation−reduction treatment at 500 K essentially resulted in the same effect as vacuum annealing at 800 K, except that the former is not accompanied by significant morphology changes (cf. Figure 1a,c).

Interestingly, the same H_2/O_2 treatment at 500 K applied to the sample preannealed to 800 K caused almost no changes in the CO TPD spectra (see Figure 2a). In the opposite sequence, when the sample is first oxidized at 500 K and then annealed to 850 K (to desorb surface oxygen[37,38]), CO uptake is reduced due to the strong particle sintering clearly seen in Figure 3a. Again, good metal/oxide epitaxy is observed as the particle edges are all parallel to the atomic rows of protrusions on the Fe_3O_4 (111) surface.

Figure 3 also shows that the top facets of the largest particles exhibit a Moiré superstructure with ∼25 Å periodicity. The more detailed structure could not be resolved in our experiments. Note, however, that an observation of oxide supported metal nanoparticles with atomic resolution is very challenging, and only a few examples are reported in the literature for encapsulating oxide layers.[11−16]Since the Moiré structure has the same periodicity as the FeO (111) monolayer film on Pt (111), resulting from ∼10% mismatch between their lattices,[30,39] we conclude that the encapsulating layer is FeO (111) in nature. It is better seen because the Moiré unit cell is comparable to the top facets' width. However, the surface of the largest particles formed at high temperatures; however, the surface of smaller particles also exhibits a weak wave-like modulation with similar periodicity.

Interestingly, very few particles reveal top facets with a lattice of protrusions, although of lower corrugation amplitude, that is identical to that resolved on the Fe_3O_4 (111) substrate between particles (Figure 3b). Since the surface of those particles also shows a Moiré-like modulation, it is unclear yet whether this structure indicates the formation of an Fe_3O_4(111) thin layer or some sort of surface (2 × 2) reconstruction of the FeO (111) overlayer previously observed by STM on the iron oxide films prepared at low temperatures.[40] Nevertheless, these are minority structures as observed.

Therefore, our STM study combined with CO TPD results provides direct evidence for the encapsulation of Pt particles once annealed to 800−850 K. To rationalize these results, we first addressed the morphology of Pt particles. As shown in Figure 1a, Pt deposits heated to 600 K in a vacuum form extended islands 2 ML in height. Note that under the same conditions, Pd forms only well-shaped 3-D particles.[25,27] Since the surface energy (γ) of Pt is higher than that of Pd,[41] which would form even more ball-like particles, the wetting behavior observed for Pt on Fe_3O_4 (111) implies a higher work of adhesion (W_{adh}), which is defined through the corresponding surface energies as

$$W_{adh} = \gamma_{oxide} + \gamma_{metal} - \gamma_{interface} \quad (1)$$

As previously shown for Pd particles supported on thin alumina films,[42] the adhesion energy can be derived from the structural information provided by STM on the basis of Wulff construction analysis of the particles that reached the equilibrium shape.[43] For metal particles, mainly exposing (100) and (111) facets, the adhesion energy can be expressed as follows (see ref 42 for the details):

$$W_{adh} = \gamma_{111}\left(2 - \frac{3}{\sqrt{2}}\frac{h}{w}\frac{s+1}{2s+1}\right) \quad (2)$$

where γ_{111} is the surface energy of the (111) surface, h (w) is height (width) of particles, and s is the ratio of the top facet side length ($s = s_{100}/s_{111}$).

For irregularly shaped Pt islands formed on Fe_3O_4 (111) at 600 K (see Figure 1a), the term "particle width" cannot be accurately defined. Moreover, the formation of extended 2-D islands, which dewet into 3-D particles upon further annealing to 800 K, may indicate that these structures are not in an equilibrium shape at 600 K. On the other hand, long-time annealing is needed for their partial transformation into 3-D particles. In addition, Figure 1a shows that the largest islands are in fact formed by the coalescence of smaller but better shaped islands, structural parameters of which can be used in the calculations. Of course, it is difficult to judge the symmetry of the edge planes, which are only two layers in height. Nonetheless, according to eq 2, for the small height/width ratios observed on Pt islands, the work of adhesion is rather insensitive

to variations in *s*. Under these assumptions, which result in a relatively large uncertainty, we obtain $W_{adh} = 4.0 \pm 0.5$ J/m^2 by using the theoretical value of 2.3 J/m^2 for $\gamma_{Pt(111)}$ as calculated by Vitos et al.[41] For 3-D particles formed at 600 K and also imaged in Figure 1a, the analysis is more precise and gives $W_{adh} = 3.8 \pm 0.1$ J/m^2. Both numbers are significantly larger than the 3.15 ± 0.1 J/m^2 value we obtained for Pd/Fe_3O_4 (111) at 600 K and the 3.25 ± 0.3 J/m^2 value previously found for Pd on thin alumina films at 300 K,[42] using the γ values for Pd (111) and Pt (111) from DFT calculations of the same group[41] for comparison.

For the particles annealed to 800 K (Figure 1b), the same approach gives $W_{adh} = 4.15 \pm 0.1$ J/m^2, which is higher than the ~3.8 J/m^2 value calculated above for 3-D particles formed at 600 K. However, one should keep in mind that the calculations were performed under the assumption that the particles expose clean Pt surfaces, which is obviously not the case at 800 K. The encapsulating oxide layer must reduce the surface energy of the particles formed at 800 K. In a crude approximation, γ_{111} used in the calculations at 600 K must be substituted by $\gamma_{FeO/Pt(111)}$ at 800 K. The latter is unknown but obviously smaller than $\gamma_{Pt(111)}$; therefore, the value 4.15 J/m^2 gives an upper limit in this case.

Thus, the previous analysis shows the high adhesion energy of Pt on Fe_3O_4 (111), which seems to favor the encapsulation of Pt particles, although the encapsulating oxide is not the same as the substrate. It is well-established that growth of iron oxide films on Pt(111) single crystals proceeds via the Stranski−Krastanov mode.[31] At 870 K, a FeO (111) overlayer grows in 10^{-6} mbar of O_2 at a coverage up to ~2 ML. At 1000 K, only a single FeO (111) layer is formed, on top of which the Fe_3O_4(111) islands grow and coalesce at increasing coverage. This means that the growth of the (O-terminated) FeO (111) layer wetting the Pt (111) surface is thermodynamically more favorable than growth of the Fe_3O_4-like islands at the same (low) Fe coverage. These results fully support our STM observation of preferential encapsulation of the Pt top facets at 850 K by the FeO (111) layer. Since FeO (111) monolayer films can be grown on the Pt (100) surface as well,[44] it seems plausible that encapsulation by the FeO (111) layer also occurs on the side facets, which mainly expose (111) and (100) surfaces as judged by observation of the hexagonally shaped particles.

Besides thermodynamic considerations favoring the SMSI effect for Pt on iron oxides, one also should consider the kinetics. Following Fu et al.,[21,22] another important factor leading to the SMSI effect is a band bending that occurs at the interface between a metal particle and an oxide support having different work functions. The work function of Pt (111) (~5.93 eV[45]) is larger than that of Fe_3O_4 (111) (~5.52 eV[30]), which exhibits a high electrical conductivity due to an electron hopping process between Fe^{2+} and Fe^{3+} at temperatures above 120 K (Verwey transition). Therefore, the contact between Pt and Fe_3O_4 must result in electron transfer from Fe_3O_4 to Pt and an upward bending of the bands in Fe_3O_4. The surface negative charges will drive the diffusion of the Fe cations toward the surface. This diffusion processes may be kinetically limited and is therefore enhanced at elevated temperatures, resulting in more pronounced encapsulation at high temperatures as shown by CO TPD (see Figure 2).

Interestingly, the Pt surface area, which is not affected by SMSI and may adsorb CO, is approximately the same, independent of whether the encapsulation is performed by vacuum annealing or by H_2/O_2 treatment. This finding suggests that encapsulation does not occur on some Pt sites. This in turn may change the selectivity of reactions through selective blocking of the reaction sites otherwise possible in the absence of encapsulation.

Conclusion

Combined STM and CO TPD results provide strong evidence for SMSI between Pt and iron oxide Fe_3O_4 supports whereby the Pt particles are primarily encapsulated by the FeO (111) monolayer film. The encapsulation most probably starts on the particle edges and first affects low coordination Pt atoms. The interaction of Pt with Fe_3O_4 (111) is found to be different from Pd on the same support studied previously. The high adhesion energy between Pt and iron oxides derived from STM data seems to be a driving force for encapsulation. This study supports the general trend that the SMSI effect is inherent to Pt when supported on reducible oxides.

Acknowledgment. We are indebted to the Deutsche Forschungsgemeinschaft, the European Community within FP6 for funding GSOMEN, the Cluster of Excellence UNICAT funded by the Deutsche Forschungsgemeinschaft and coordinated by the Technical University Berlin, and to Fonds der Chemischen Industrie for financial support.

References and Notes

(1) Tauster, S. J.; Fung, S. C.; Garten, R. L. *J. Am. Chem. Soc.* **1978**, *100*, 170.
(2) Haler, G. L.; Resasco, D. E. *Adv. Catal.* **1989**, *36*, 173.
(3) Henrich, V. *Rep. Prog. Phys.* **1985**, *48*, 1481.
(4) Solymosi, F. *J. Catal.* **1985**, *94*, 581.
(5) Datye, A. K.; Kalakkad, D. S.; Yao, M. H.; Smith, D. J. *J. Catal.* **1995**, *155*, 148.
(6) Knözinger, H.; Taglauer, E. In *Handbook of Heterogeneous Catalysis*; Ertl, G., Knözinger, H., Weitkamp, J., Eds.; VCH: Weinheim, Germany, 1997; p 216.
(7) Pesty, F.; Steinrück, H.-P.; Madey, T. E. *Surf. Sci.* **1995**, *33*, 9–83.
(8) Pan, J.-M.; Madey, T. E. *Catal. Lett.* **1993**, *20*, 269.
(9) Cosandey, F.; Zhang, L.; Madey, T. E. *Surf. Sci.* **2001**, *474*, 1.
(10) Suzuki, T.; Souda, R. *Surf. Sci.* **2000**, *448*, 33.
(11) Dulub, O.; Hebenstreit, W.; Diebold, U. *Phys. Rev. Lett.* **2000**, *84*, 3646.
(12) Jennison, D. R.; Dulub, O.; Hebenstreit, W.; Diebold, U. *Surf. Sci.* **2001**, *492*, 677.
(13) Bennett, R. A.; Stone, P.; Bowker, M. *Catal. Lett.* **1999**, *59*, 99.
(14) Bowker, M.; et al. *J. Catal.* **2005**, *234*, 172.
(15) Bowker, M.; Stone, P.; Bennett, R.; Perkins, N. *Surf. Sci.* **2002**, *497*, 155.
(16) Silly, F.; Castell, M. R. *J. Phys. Chem. B* **2005**, *109*, 12316.
(17) Sedona, F.; Agnoli, S.; Granozzi, G. *J. Phys. Chem. B* **2006**, *110*, 15359.
(18) Mullins, D. R.; Zhang, K. Z. *Surf. Sci.* **2002**, *513*, 163.
(19) Senanayake, S. D.; Zhou, J.; Baddorf, A. P.; Mullins, D. R. *Surf. Sci.* **2007**, *601*, 3215.
(20) Gao, Y.; Liang, Y.; Chambers, S. A. *Surf. Sci.* **1996**, *365*, 638.
(21) Fu, Q.; Wagner, T.; Olliges, S.; Carstanjen, H.-D. *J. Phys. Chem. B* **2005**, *109*, 944.
(22) Fu, Q.; Wagner, T. *Surf. Sci. Rep.* **2007**, *62*, 431.
(23) Gatel, C.; Snoeck, E. *Surf. Sci.* **2006**, *600*, 2650.
(24) Gatel, C.; Snoeck, E. *Surf. Sci.* **2007**, *601*, 1031.
(25) Meyer, R.; Shaikhutdinov, S.; Freund, H.-J. *Z. Phys.* **2004**, *218*, 905.
(26) Schalow, T.; et al. *Surf. Sci.* **2006**, *600*, 2528.
(27) Schalow, T.; et al. *Catal. Lett.* **2006**, *107*, 189.
(28) Schalow, T.; et al. *J. Catal.* **2006**, *242*, 58.
(29) Schalow, T.; et al. *Angew. Chem., Int. Ed.* **2005**, *44*, 7601.
(30) Weiss, W.; Ranke, W. *Prog. Surf. Sci.* **2002**, *70*, 1.
(31) Weiss, W.; Ritter, M. *Phys. Rev. B: Condens. Matter Mater. Phys.* **1998**, *59*, 5201.
(32) Lemire, C.; Henrich, V.; Shaikhutdinov, S.; Freund, H.-J. *Surf. Sci.* **2004**, *572*, 103.
(33) McCabe, R. W.; Schmidt, L. D. *Surf. Sci.* **1977**, *66*, 101.
(34) Ertl, G.; Neumann, M.; Streit, K. M. *Surf. Sci.* **1977**, *64*, 393.
(35) Steiniger, H.; Lehwald, S.; Ibach, H. *Surf. Sci.* **1982**, *123*, 264.
(36) Mcclellan, M. R.; Gland, J. L.; McFesly, F. R. *Surf. Sci.* **1981**, *112*, 63.

(37) Putna, E. S.; Vohs, J. M.; Gorte, R. J. *Surf. Sci.* **1997**, *391*, 1178.
(38) Zhu, X.-Y.; Hatch, S. R.; Campion, A.; White, J. M. *J. Chem. Phys.* **1989**, *91*, 5011.
(39) Vurens, G. H.; Maurice, V.; Salmeron, M.; Somorjai, G. A. *Surf. Sci.* **1992**, *268*, 170.
(40) Shaikhutdinov, S.; Ritter, M.; Wang, X. G.; Over, H.; Weiss, W. *Phys. Rev. B: Condens. Matter Mater. Phys.* **1999**, *60*, 11062.
(41) Vitos, L.; Ruban, A.; Skriver, H.; Kollár, J. *Surf. Sci.* **1998**, *411*, 186.
(42) Hansen, K. H.; et al. *Phys. Rev. Lett.* **1999**, *83*, 4120.
(43) Wulff, G. *Z. Kristallogr.* **1901**, *34*, 449.
(44) Shaikhutdinov, S.; Ritter, M.; Weiss, W. *Phys. Rev. B: Condens. Matter Mater. Phys.* **2000**, *62*, 7535.
(45) Weast, R. C.; Astle, M. J. *CRC Handbook of Chemistry and Physics*, 63rd ed.; CRC Press: Boca Raton, FL, 1982.

JP801756Q